

BINOL–Amino Acid Conjugates as Triggerable Carriers of DNA-Targeted Potent Photocytotoxic Agents

Filippo Doria,^{†,‡} Sara N. Richter,^{§,‡} Matteo Nadai,[§] Stefano Colloredo-Mels,[†] Mariella Mella,[†] Manlio Palumbo,^{||} and Mauro Freccero^{*,†}

Dipartimento di Chimica Organica, Università di Pavia, V. le Taramelli 10, 27100 Pavia, Italy, Dipartimento di Istologia, Microbiologia e Biotecnologie Mediche, Università di Padova, via Gabelli, 63, 35121, Padova, Italy, and Dipartimento di Scienze Farmaceutiche, Università di Padova, Via Marzolo, 5, 35131 Padova, Italy

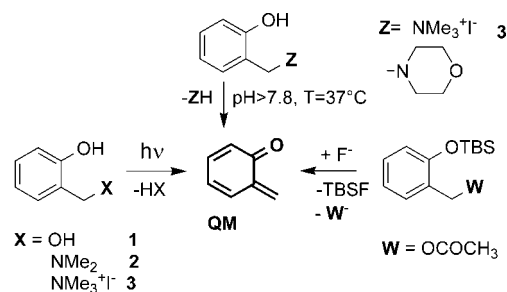
Received July 9, 2007

Mild photoactivation of new BINOL–amino acid and –amino ester conjugates (BINOLAMs) yielded alkylating and DNA cross-linking agents with high photoefficiency and superior cytotoxicity. Detection of the transient electrophile, by laser flash photolysis (LFP), suggests that BINOL–quinone methides (QMs) are key intermediates in the process. QMs trapping by water, monitored in a time-dependent product distribution analysis, demonstrated that the phototriggered reactivity of BINOLAMs as bis-alkylating agents is the result of a two-step process involving sequential photogeneration of monoalkylating QMs. Light activation of the BINOL–L-amino esters produced cytotoxic QMs very effective against human tumor LoVo cells with EC₅₀ in the 130–230 nM range. Trimethylpsoralen (PS) is about 4 times less potent than our newly tested compounds. BINOL–L-proline methyl ester showed notable photoselectivity because it displayed cytotoxic effects upon irradiation only and was able to efficiently reach the target DNA inside the cells, where it forms both alkylated and cross-linked species.

Introduction

Several strategies have been devised and developed for the selective and mild activation of DNA-modifying agents. The generation of reactive intermediates, starting from stable precursors, with DNA-binding properties, has great potential for the development of chemotherapeutic prodrugs¹ and for the investigation and understanding of DNA–protein interactions.² Therefore, it is not surprising that advances in areas of oxidative, reductive, hydrolytic, and photochemical activation protocols continue to generate promising and clinically relevant agents.³ Among them, the phototriggerable cleaving^{1b,4} and alkylating/cross-linking^{1a,b,4} agents have attracted a great deal of attention in the past decade, mainly because, contrary to most nonphotochemically activable DNA-modifying agents, they do not require a coreagent under conditions not always compatible with *in vivo* applications.⁴ Although in the recent past a wide variety of photochemically activated DNA reactive agents have been discovered and investigated, they mainly act as cleavers involving radical reactive intermediates. Fairly limited examples of photochemically activated DNA-alkylating agents have been reported.⁵ In fact, to date, psoralens are the only well-established class of drugs known to induce DNA or RNA cross-linking upon photoactivation.⁶ Recently, our research has been focused on another class of reagents that similarly express a triggerable ability to alkylate nucleic acids through the generation of highly reactive quinone methides (QMs)^a (Scheme 1).⁷

Scheme 1. Photochemical and Thermal (Fluoride and pH-Induced) Generation of the Prototype QM



These electrophilic intermediates have been generated by photochemical^{5,7–10} and thermal^{7a,11–13} (fluoride and pH-induced) mild activation procedures. In both cases, the generation of a phenolate, by excited-state proton transfer¹⁴ or by fluoride-induced desilylation,^{11–13} is the key mechanistic step leading to the electrophilic QMs. QMs, particularly those with an *ortho* geometry (*o*-QMs), have been successfully used to accomplish amino acid,^{7a} oligopeptide,^{7a} nucleoside mono- and bis-alkylations,^{11,12} and DNA-cross-linking^{5,7b,15} in water (according to the sequence reported in Scheme 2). In more detail, Wan,^{8,14} Kresge,⁹ Saito,¹⁰ Zhou,^{15b} and our group⁷ described the photogeneration of QMs starting from benzyl alcohols (**1**, Scheme 1),^{8,9} Mannich bases (**2**, Scheme 1),^{7,10} and their quaternary ammonium salts (**3**, Scheme 1) in water.^{7,15b} These reactive intermediates, with tunable electrophilicity by substituent effects,¹³ have also been trapped by biological nucleophiles and detected by nanosecond laser flash photolysis (LFP).^{7a–e,8,9}

Recently, we have also shown that BINOL derivatives, such as the bis-quaternary ammonium salt **3b**, are capable of undergoing bis-alkylation in water and DNA cross-linking with promising potency by UV–vis photoactivation (Scheme 3).^{7b}

Furthermore, unlike precursors **1–3**, the quaternary ammonium salts **3a** and **3b** exhibit high absorptivity at a wavelength longer than 360 nm and excellent solubility under

* To whom correspondence should be addressed: Università di Pavia, Dipartimento di Chimica Organica V. le Taramelli 10, 27100 Pavia, Italy. Telephone: +39-0382-987668. Fax: +39-0382-987323. E-mail: mauro.freccero@unipv.it.

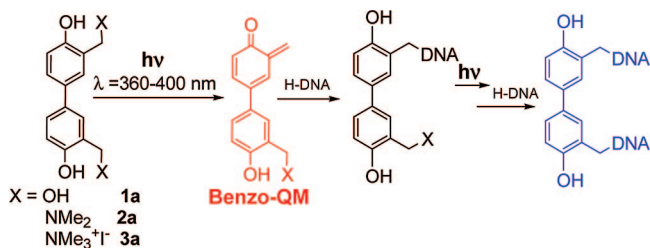
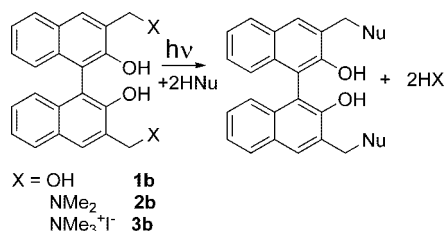
[†] Università di Pavia.

[‡] These authors contributed equally to this work.

[§] Dipartimento di Istologia, Microbiologia e Biotecnologie Mediche, Università di Padova.

^{||} Dipartimento di Scienze Farmaceutiche, Università di Padova.

^a Abbreviations: QMs, quinone methides; BINOLAM, BINOL–amino acid and –amino ester conjugate; PS, 4,5',8-trimethylpsoralen; LFP, laser flash photolysis; XL, cross-linking.

Scheme 2. Benzo-QMs Photogeneration and Reactivity as Alkylating and DNA Cross-Linking Agents**Scheme 3.** Photoactivation of BINOL Derivatives as Bis-alkylating Agents

physiological conditions, which are considered the basic requirements for useful DNA-alkylating agents. Unfortunately, the binol derivatives **1a(b)**–**3a(b)** exhibit severe limitations for *in vivo* applications because of the presence of the permanently charged quaternary ammonium moieties, which prevent binols from crossing biological membranes. Contrary, the phototriggerable BINOL unit tethered to amino acid derivatives and oligonucleotides could be characterized by adequate cell permeability¹⁶ and biological target recognition properties,¹⁷ respectively. Here, we describe the first step toward BINOL–oligopeptide conjugates as selective and triggerable carriers of bifunctional BINOL–QMs targeting DNA. We report the synthesis, photoreactivity, DNA cross-linking properties, and photocytotoxicity of rational BINOL–amino acid derivatives (BINOLAMs). Indeed, the novel derivatives represent valuable lead compounds for selective cellular DNA-damaging activity.

Results and Discussion

The target compounds investigated in the current study are 3,3′-bis-CH₂Y-substituted BINOLs represented by the general structure, highlighted in red in Chart 1.

They all contain two CH₂Y arms on the BINOL moiety, which act as absorbing chromophores for the activation of the BINOLAMs by photoinduced HX elimination. Compounds **4–10** (Chart 1) differ from each other by the Y group structure, which was chosen among N-substituted L-amino acids and related amino esters, with or without basic side-chain groups: L-proline (**4**, **5**, and **6**), L-alanine (**7**), L-valine (**8**), and L-lysine (**9** and **10**). The Y moiety structures were selected for the following reasons: (a) organic molecules exhibiting net positive charges under physiological conditions should exhibit enhanced DNA binding through electrostatic interactions with the polyanionic backbone of the nucleic acid; (b) the spacer length could modulate the binding properties of the precursors; (c) the protonation–deprotonation equilibria in the amino acid derivatives should remarkably improve cell permeability of the new BINOL conjugates in comparison to that of the fully charged quaternary ammonium salts (**3a** and **3b**), previously investigated as DNA cross-linking agents.^{7b} The role as chiral ligands in the modern enantioselective catalysis of BINOL derivatives¹⁸ propelled us to exploit the robust chemistry of the BINOLs to

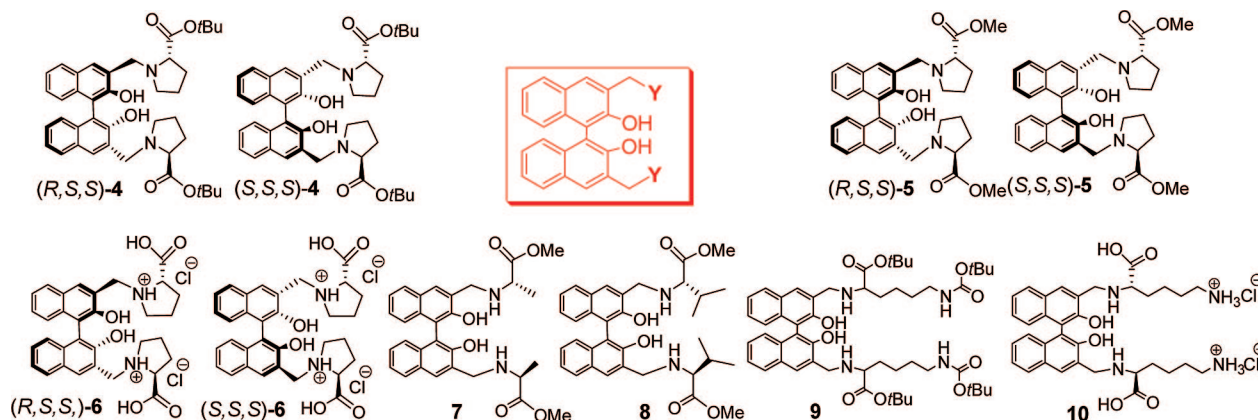
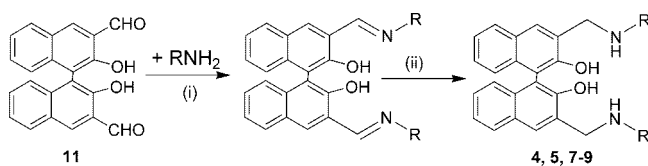
prepare new diastereomerically pure BINOLAMs **4–6** and enantiopure BINOLs **3a–3c**. These allowed us to explore possible diastereo- and enantioselectivity effects on DNA cross-linking potency and photocytotoxicity/cytotoxicity properties of the BINOLAMs.

Synthesis of BINOL–Amino Acid Conjugates. The BINOLAMs **4–10** investigated as a phototriggerable source of bis-alkylating species were synthesized mainly by a reductive amination reaction,¹⁹ using the dialdehyde **11**²⁰ in a stepwise approach with the preformation of the intermediate imine, and further reduction in a separate step (Scheme 4).

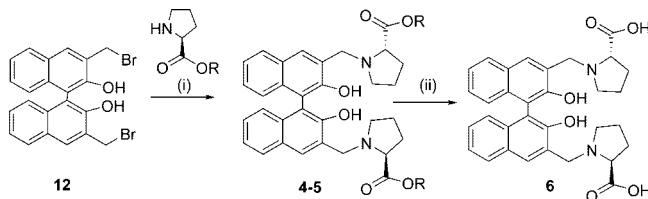
After surveying many of the commercially available hydride reagents, we selected sodium triacetoxyborohydride [NaBH(OAc)₃] based on the resulting overall reductive amination reaction yields (always higher than 85%). Imine preformation was achieved adding the dialdehyde **11** to L-alanine-OMe, L-valine-OMe, L-proline-OMe, L-proline-OtBu, and N-ε-*t*-butyloxycarbonyl-L-lysine-*t*-butyl ester in anhydrous CH₂Cl₂ and 4 Å molecular sieves. The diastereomeric L-diprolino esters (*S,S,S*)- and (*R,S,S*)-**4** and **-5** and their related amino acid **6** were also synthesized starting from the BINOL–3,3′-bis-CH₂Br (**12**) in higher yields (according to Scheme 5) or following an original photochemical protocol optimized by our group, starting from racemic BINOLAM **2b**.^{7c}

In both cases, a 1:1 diastereomeric mixture was obtained. The (*S,S,S*)-**4** and (*S,S,S*)-**5** adducts were the first, among the two diastereoisomers, to be eluted from preparative column chromatography (7:3 cyclohexane/ethyl acetate), with very good diastereomeric excess (de) ≥ 99%. Crystallization of the diastereomeric mixture from benzene and ethyl acetate afforded the (*S,S,S*) and (*R,S,S*) pure isomers, respectively, with a slightly lower purity (de ≤ 95%). The absolute configurations of (*R,S,S*)-**4**, (*S,S,S*)-**4**, (*R,S,S*)-**5**, and (*S,S,S*)-**5** were assigned by a comparison to authentic samples synthesized quantitatively starting from chiral (*R*)- and (*S*)-dibromide **12** and proline methyl and *t*-butyl esters, respectively (Scheme 5). The BINOL–amino acid conjugates (**6** and **10**) were quantitatively prepared starting from the *t*-butyl esters, following the standard deprotection protocol (TFA, Et₃SiH, and CH₂Cl₂ at room temperature for 25 min).²¹

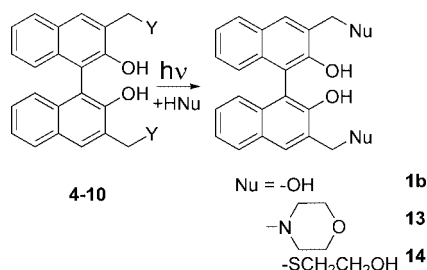
BINOL–Amino Acid and Ester Conjugates as Phototriggerable Bis-alkylating Agents. To test **4–10** as phototriggerable precursors of bis-alkylating QMs, we first explored the photoreactivity of **4–6** as pure diastereoisomers and **7**, **8**, and **10** as 1:1 diastereomeric mixtures. The BINOL–QMs were photogenerated both at 310 and 360 nm wavelengths and trapped by water, morpholine, and 2-mercaptoethanol (Scheme 6), in buffered (pH 7.5) 1:1 H₂O/CH₃CN. In more detail, photolysis of diastereomerically pure (*S,S,S*)- and (*R,S,S*)-**4–6**, in the absence of an added nucleophile, gives the alcohol (*R*)- and (*S*)-**1b**, respectively, in quantitative yields, with complete retention of the BINOL-moiety configuration (after 10 min of irradiation). Photolysis of **4–6** in a water solution containing morpholine and mercaptoethanol similarly afforded the bis-morpholino adduct **13** and the bifunctional thioether **14**, in good yields, accompanied by small amounts (<15%) of alcohol **1b**. Fairly similar conversion rates were achieved with the BINOL–L-valine-OMe ester (**8**) and the BINOL–L-lysine (**10**). The only exception to this trend was due to BINOL–alanine-OMe ester (**7**), which turned to be much less reactive, requiring a longer irradiation time (10 min) and yielding a lower conversion (lower than 35%, see the Supporting Information for detailed information). Monoalkylated adducts were not detected by high-performance liquid chromatography (HPLC) under the reaction

Chart 1. BINOL–Amino Acid Derivatives (**4–10**) Synthesized and Tested as Photocytotoxic Bis-alkylating Agents**Scheme 4.** Synthetic Protocol for the BINOLAMs **4**, **5**, and **7–9**^a

^a (i) Molecular sieves at 4 Å in CH₂Cl₂; (ii) NaBH(OAc)₃, CH₂Cl₂, and N₂.

Scheme 5. Synthesis of BINOL–Diprolino Derivatives **4–6**^a

^a (i) K₂CO₃, CH₂Cl₂, Δ, 5 h. (ii) TFA, Et₃SiH, CH₂Cl₂, room temperature, 25 min.

Scheme 6. Photoreactivity of BINOLAMs **4–10** in Water, 10^{−3} M, in a Merry-go-round Photoreactor, with 4 Lamps at 15 W, 310 and 360 nm; ca. 25 °C, 15 and 40 min, Respectively, and N₂ Purged

conditions described above, and if formed, their yields were lower than 5%.

Mechanistic Insights from Time-Dependent Product Distribution Analysis and Quantum Yield Measurements.

We have shown that the photoactivation of adducts **4–10** as bifunctional alkylating agents is a general key feature of the BINOLAMs. Therefore, considering worthwhile the investigation of its mechanism, we run three sets of clarifying experiments: (i) monitoring the photohydration process by time-dependent product distribution analysis, (ii) evaluating the photochemical efficiency by quantum yield measurements, and (iii) detecting the electrophilic transient by LFP. Running the

photochemical reaction of (*S,S,S*)- and (*R,S,S*)-**6** under low conversion (<40%) conditions, achievable for short irradiation times (0.5–5 min, in a merry-go-round photoreactor, with 2 lamps at 15 W, 310 nm; ca. 25 °C, and N₂ purged), it was clear that the monohydrated intermediates [(*S,S*)- and (*R,S*)-**15**; see Figure 1] were formed first and subsequently reacted to give alcohols (*S*)-**1b** and (*R*)-**1b**, respectively. The profile of the converted precursor (*S,S,S*)-**6** into the intermediate monohydrated adduct (*S,S*)-**15**, toward the final product (*S*)-**1b**, as a function of the irradiation time is reported in Figure 1a. A similar time-dependent product distribution analysis was run for the diastereoisomer (*R,S,S*)-**6** (Figure 1b).

The monohydrated adducts (*S,S*)-**15** and (*R,S*)-**15** were formed rapidly, reaching a maximum yield after 4–5 min of irradiation (Figure 1). Photoinduced decomposition of the resulting adducts was also rapid, with 80–90% conversion of the starting material into alcohols (*S*)-**1b** and (*R*)-**1b** within 15 min (Figure 1). A closer comparison of the two product profiles in Figure 1a and 1b reveals that the diastereoisomer (*R,S,S*)-**6** is slightly more photoreactive than (*S,S,S*)-**6**. Such a difference is confirmed by quantum yield measurements (Table 2). In fact, irradiation of (*R,S,S*)-**6** generates the monohydrated adduct (*R,S*)-**15**, with a 56% conversion after 4 min of irradiation, and the irradiation of (*S,S,S*)-**6** generates the monohydrated adduct (*S,S*)-**15**, with a 37% conversion after the same irradiation time. In a comparable fashion, we have monitored the product distribution as a function of the irradiation time also for the *L*-proline *t*-butyl esters [(*R,S,S*)-**4** and (*S,S,S*)-**4**] in a 1:1 acetonitrile/water solution. In this case, both (*R,S*)-**16** and (*S,S*)-**16** resulting from the monohydration process reached a maximum after 7 min and no measurable difference in the photoreactivity between the diastereoisomers was recorded.

These time-dependent profiles, displaying the trend of reactant (**6**) consumption, intermediates (**15**), and final product formation (**1b**) of the hydration process, demonstrate that the BINOL–amino ester and BINOL–amino acid conjugates (**4** and **6**, respectively) both act as phototriggerable bis-alkylating agents through the sequential generation of two monoalkylating quinone methides. In addition, adduct (*R,S,S*)-**6** exhibits a slightly higher efficiency in the photogeneration of the monohydration adduct in comparison to its diastereoisomer (*S,S,S*)-**6**. To evaluate the photoefficiency of the BINOL–amino acids and BINOL–amino esters (**4–8**) in the generation of alkylating QMs, we also measured their quantum yields, comparing them to other photoreactive BINOLs, including the monohydrated adducts **15** and **16**. The measured quantum yields are listed in Table 1.

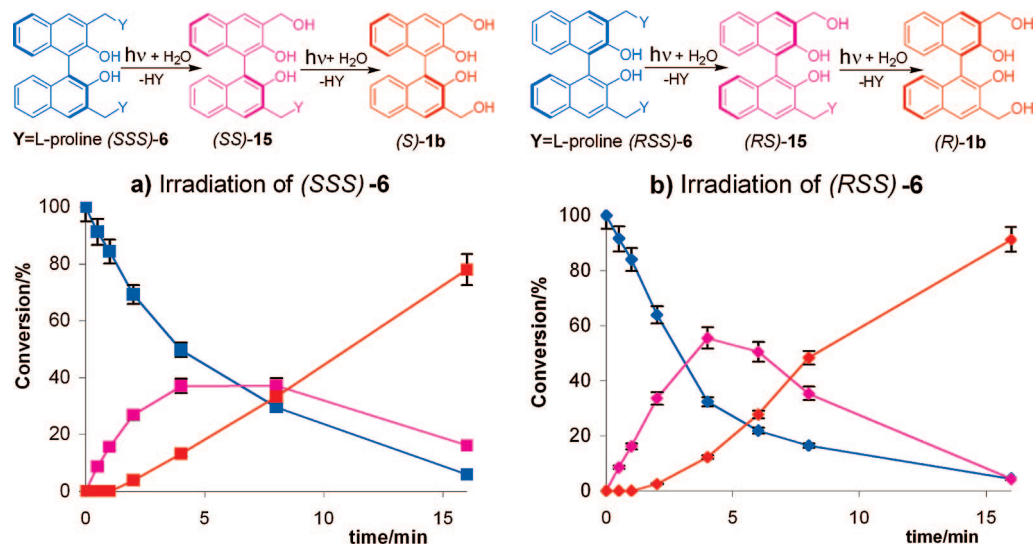


Figure 1. Product distribution dependence on the irradiation dose, for the irradiation of (*S,S,S*)-**6** (a) and (*R,S,S*)-**6** (b).

Table 1. Quantum Yields (Φ)^a of the BINOL–QM Photochemical Generation, Measured in 1:1 H₂O/CH₃CN Solutions of the BINOLAMs (3×10^{-4} M) at Low Conversion (<30%), under Buffered Conditions (Phosphate Buffer, 10^{-2} M, pH 7.5)

BINOLAMs	Φ ^a
1b ^b	0.47 (± 0.05) ^c
3b ^b	0.70 (± 0.04) ^d
(<i>S,S,S</i>)- 4	0.24 (± 0.02) ^d
(<i>R,S,S</i>)- 4	0.28 (± 0.06) ^d
(<i>S,S,S</i>)- 6	0.43 (± 0.04) ^d
(<i>R,S,S</i>)- 6	0.60 (± 0.06) ^d
7 ^e	0.05 (± 0.01)
8 ^e	0.62 (± 0.05)
(<i>S,S</i>)- 15	0.94 (± 0.06) ^f
(<i>R,S</i>)- 15	0.95 (± 0.05) ^f
(<i>S,S</i>)- 16	0.90 (± 0.04) ^f
(<i>R,S</i>)- 16	0.93 (± 0.08) ^f

^a By potassium ferrioxalate actinometry (monitored by UV–vis). ^b Racemate. ^c Quantum yield for the formation of **15** for Y = morpholino, using morpholine 5×10^{-2} M as a trap. ^d Quantum yield for the formation of monohydrated adducts, such as **15**. ^e As a 1:1 diastereomeric mixture. ^f Quantum yield for the formation of **1b**.

Table 2. Biological *in Vitro* and Cellular Properties of BINOL–Amino Acid Conjugates

QM	DNA XL MC (μ M)	EC ₅₀ (μ M)	CC ₅₀ (μ M)	SI (CC ₅₀ /EC ₅₀)	log P
PS	<0.5	0.94 \pm 0.09	>200	>210	2.44
(<i>S</i>)- 3b	1.25	>200	>200		ionic
(<i>R</i>)- 3b	1.25	>200	>200		
(<i>S,S,S</i>)- 5	20	0.22 \pm 0.05	>200	>900	4.81
(<i>R,S,S</i>)- 5	20	0.23 \pm 0.02	>200	>860	
(<i>S,S,S</i>)- 6	2.5–5	>200	>200		4.28
(<i>R,S,S</i>)- 6	2.5–5	>200	>200		
7	>40	4.00 \pm 0.8	1.5 \pm 0.2	0.4	4.38
8	5	0.13 \pm 0.04	14.0 \pm 6.0	108	6.15
10	20	>200	>200		3.34

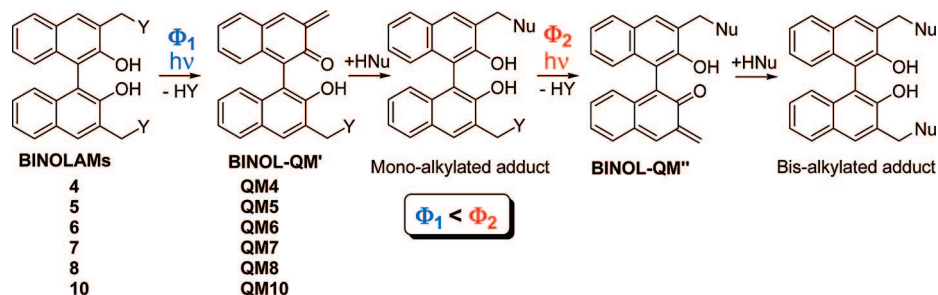
All BINOLAMs act as efficient photoalkylating agents. In general, with the exception of the BINOL–L-alanine-OMe ester (in agreement with the preparative experiment results), the quantum yield is higher than 0.24 and reaches its maximum for the monohydrated adduct **15** ($\Phi > 0.9$). Among them, the monohydrated amino acid and *t*-butylester derivatives (*S,S*)- and (*R,S*)-**15** and **-16** are the most efficient, followed by the quaternary ammonium salts (*S*)- and (*R*)-**3b** and the BINOL–valine methyl ester **8**. The quantum yield is a function of the amino acid/ester moieties and conformational aspects, because

the diastereoisomers (*R,S,S*)-**4** and **-6** are slightly more efficient as photoalkylating agents than their related (*S,S,S*) diastereoisomers. The highest efficiency of **15** and **16** as photoalkylating agents explains why, in the preparative experiments run with 4 lamps for 15 min, (a) only bis-alkylated adducts were isolated and (b) the detection of the monohydrated products (**15** and **16**) was possible only in short irradiation experiments (<10 min, using 2 lamps only).

Detection of Monoalkylating BINOL–QM by LFP. LFP provides a general and effective method for direct UV–vis detection of transient QMs starting from *o*-hydroxybenzylic alcohols, as clearly demonstrated by the extensive work of Wan's^{8–14} and Kresge's groups.⁹ More recently, we have displayed that similar results can be achieved starting from Mannich bases (**2**) and their quaternary ammonium salts (**3**).^{9,11,15} In more detail, LFP of **2b** and **3b**, in water and 1:1 water/acetonitrile solutions, generates monoalkylating BINOL–QM as transient species, with the maximum absorbance (λ_{\max}) centered at 380 nm.^{7b} In a comparable fashion, LFP photoactivation of the BINOLAMs **4–8** and **10** at 266 and 354 nm (using a Nd:YAG laser, <10 mJ per pulse in oxygen-purged aqueous solutions) yielded transient species with very similar absorbance. The only difference detected was the intensity of the transient absorption immediately after the laser pulse, which parallels the quantum yield trend reported in Table 1. These transients were confidently assigned to the BINOL–QM structures **QM4–QM8** and **QM10** (Scheme 7) based on (i) the spectroscopic similarity of their transient spectra to that previously assigned to the BINOL–QM rising from **2b** (Scheme 2), (ii) the similar maximum absorbance of the parent 2,3-naphtho-QM ($\lambda_{\max} = 395.5$ nm),²² and (iii) trapping experiment results. In fact, after 20–30 laser shots (8 mJ power), (*S,S*)- and (*R,S*)-**15** were detected as the main products by HPLC in flashed aqueous solutions of (*S,S,S*)- and (*R,S,S*)-**6**, respectively.

In summary, the results from product distribution, time-dependent product analysis, quantum yield measurements, and LFP experiments safely indicate that BINOLAMs are bis-alkylating agents, which are efficiently phototriggerable through the sequential generation of two monoalkylating QMs, according to Scheme 7. Interestingly, the efficiency (measured by the quantum yield, Φ) in the generation of the second QM (BINOL–QM'', Φ_2) was always higher than that associated to the first one (BINOL–QM', Φ_1). These results suggest that

Scheme 7. Sequential Photogeneration of Two Monoalkylating BINOL-QMs



the BINOLAMs may act as photoactivatable mono- and bis-alkylating agents.

DNA Cross-Linking. The DNA–DNA cross-linking ability of compounds (*S*)-**3b**, (*R*)-**3b**, (*S,S,S*)-**5**, (*R,S,S*)-**5**, (*S,S,S*)-**6**, (*R,S,S*)-**6**, **7**, **8**, and **10** was investigated using a negatively supercoiled plasmid DNA (pBR322) in an alkaline agarose gel assay (Figure 2).^{7b} Compounds (*S,S,S*)-**4**, (*R,S,S*)-**4**, and **9** were not included because of their low solubility in aqueous solution. DNA cross-linking (XL) experiments were carried out in 50 mM phosphate-buffered solutions at pH 7.5. Samples were irradiated at 360 nm for 20 min. Each compound was used at increasing concentrations (0.62–80 μM , lanes 1–8 in Figure 2). Irradiated DNA without substrates (lanes D) or with PS (lanes PS) were used as controls.

The nonreacted plasmid was present in its supercoiled (*S*), linear (*L*), and nicked (*N*) forms. Interstrand cross-linking activities of tested compounds were evident as a XL band (XL), which run slightly slower than the linear form (Figure 2). Activities were measured as the minimal compound concentration (DNA XL MC) required to obtain XL effects (Table 2).

XL activities were measured for the two enantiomers *S* and *R* of compound **3b** and diastereoisomers *S,S,S* and *R,S,S* of compounds **5** and **6**. Compounds (*S*)-**3b** and (*R*)-**3b** induced detectable XL at concentrations as low as 1.25 μM [lanes 2–8

in Figure 2, QM (*S*)-**3b** and (*R*)-**3b**]. These data are in total agreement with previous results obtained with the racemic mixture of BINOL–QM **3b**.^{7b} Diastereoisomers **6** were only slightly less active than **3b**; XL effects were evident at 2.5–5 μM [lanes 3–8 in Figure 2, (*S,S,S*)-**6** and (*R,S,S*)-**6**]. BINOL derivatives **5** were around 5–8-fold less potent than **6**, because they displayed detectable XL only at a 20 μM concentration [lanes 6–8 in Figure 2, QM (*S,S,S*)-**5** and (*R,S,S*)-**5**]. No significant differences in XL potency were found between the two enantiomers (*S*)-**3b** and (*R*)-**3b** or diastereoisomers (*S,S,S*)-**6** and (*R,S,S*)-**6** of each active compound (compare lanes 3–8 in Figure 2), indicating the absence of detectable enantio- or diastereoselectivity in the DNA photo-cross-linking activity by these BINOL derivatives.

On the basis of these results, compounds **7**, **8**, and **10** were tested as racemic mixtures. Of these, BINOL derivative **8** was the most active, with a DNA XL MC of 5 μM (lanes 4–8 in Figure 2). Compounds **7** and **10** resulted less potent, being active at concentrations of 40 and 20 μM , respectively. In addition, in the presence of high concentrations of these two latter compounds (80 μM), unreacted DNA amounts decreased, without corresponding XL formation. This likely indicates the unspecific reaction of BINOL derivatives **7** and **10** with material used for handling after photoirradiation.

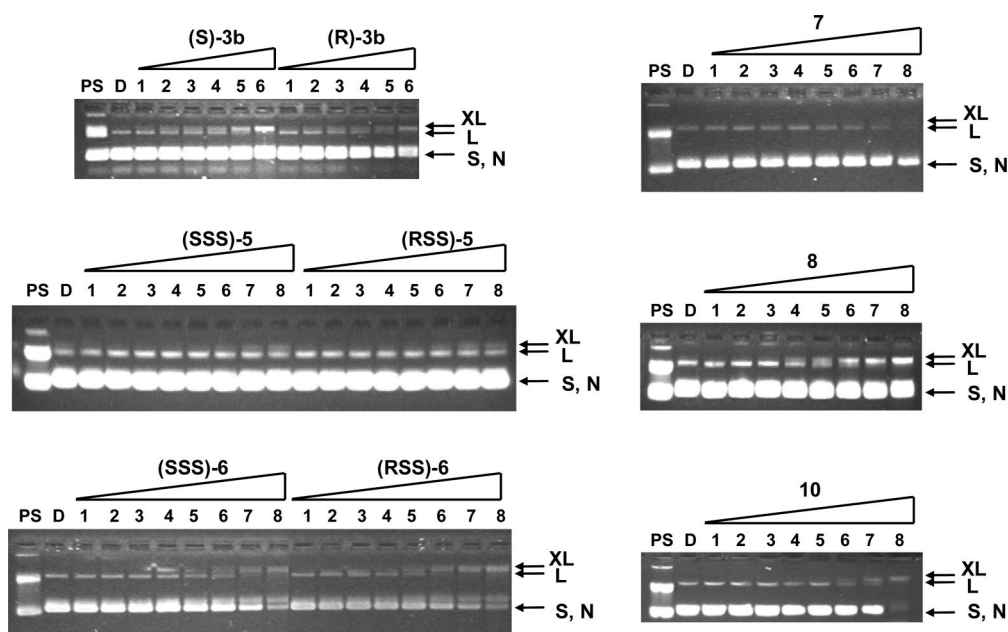


Figure 2. DNA cross-linking (XL) concentration-dependent activity of BINOL–amino acid conjugates. Plasmid DNA was mixed with increasing amounts (0.62, 1.25, 2.5, 5, 10, 20, 40, and 80 μM , lanes 1–8) of each compound (shown above each gel image), in phosphate buffer (50 mM, pH 7.5). Reaction mixtures were irradiated at 360 nm for 20 min and loaded on a 1% alkaline agarose gel. Gels were stained with ethidium bromide. Lane D is nontreated, irradiated DNA. Lane PS is a control for XL species induced by 4,5',8-trimethylpsoralen at 360 nm. Nonreacted supercoiled, nicked, and linear forms of plasmid are indicated as S, N, and L. XL species are indicated as XL, on the right of each gel image.

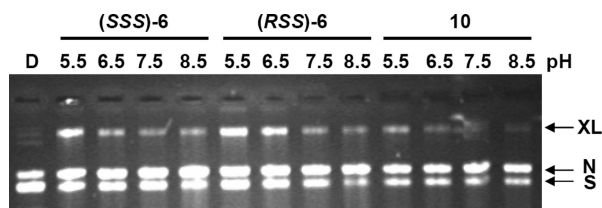


Figure 3. pH dependence activity of compounds (*S,S,S*)-**3b**, (*R,S,S*)-**3b**, and **10**. Plasmid DNA with 20 mM of indicated QMs was irradiated at 360 nm in phosphate buffer at pH 5.5, 6.5, 7.5, and 8.5. Lane D is nontreated, irradiated DNA. Nonreacted forms of plasmid are indicated as S and N. XL species are indicated as XL, on the right of each gel image.

It is noteworthy that none of the tested compounds modified DNA in the absence of photoactivation (data not shown).

Our results clearly indicate that cross-linking activity depends upon three counter-balancing properties of BINOL–QM precursors: (1) efficiency of the primary photoactivation step, (2) percentage of BINOL derivative in the bis-cationic form, (3) presence of bulky substituents. The effect of the photoactivation efficiency is obviously very important, as highlighted by the less potent XL BINOL derivative **7**, which is mainly the result of its lowest photochemical quantum yield. Concerning the effect of the net charge on the precursors, we have already reported that bis-cationic forms of QMs induce electrostatic pre-association of the QM precursors to the ionic DNA phosphate backbone, hence enhancing a subsequent covalent reaction.^{7b} In fact, XL efficiency increased when performing reactions in acid solutions, where the percentage of bis-cationic forms are enhanced. As shown in Figure 3, XL bands increased steadily from pH 8.5 to 5.5 in the presence of 20 μ M of compounds (*S,S,S*)-**6**, (*R,S,S*)-**6**, and **10**. All other BINOL–amino acid conjugates displayed a similar behavior in this range of pH (data not shown). On the other hand, bulky nonionic moieties may both mask positive charges or hinder an effective interaction between reactive groups, hence modulating cross-linking efficiency.

As demonstrated by the quantum yield measurements and LFP experiments, BINOLAMs are able to form both mono- as well as bis-alkylated and XL species. To visualize alkylation, reaction mixtures were treated for 24 h at room temperature in alkaline agarose gel buffer, prior to loading onto alkaline agarose gels. Alkaline denaturing conditions destabilize alkylated bases, thus inducing DNA scissions.²³ As shown in Figure 4, at increasing concentrations of compounds (*S*)-**3b** and (*R*)-**3b**, the band corresponding to XL species augmented up to a drug concentration of 10 μ M (lanes 1–5 in Figure 4). However, at higher drug concentrations (20–160 μ M), the XL band decreased and converted to a smeared band, comprising species running faster than the XL band itself and SC DNA as well (lanes 6–9 in Figure 4). A similar behavior was obtained with all tested BINOLAMs (data not shown). Importantly, the control PS in these conditions did not induce DNA-strand scission. These results indicate that the XL species formed by BINOLAMs but not by PS are alkali-sensitive.

Evaluation of BINOL–Amino Acid Conjugates Photocytotoxicity versus Cytotoxicity. Photocytotoxic and cytotoxic effects of BINOL–amino acid conjugates (*S*)-**3b**, (*R*)-**3b**, (*S,S,S*)-**5**, (*R,S,S*)-**5**, (*S,S,S*)-**6**, (*R,S,S*)-**6**, **7**, **8**, and **10** were investigated on the epithelial-like human colorectal adenocarcinoma LoVo cell line. This is an established cell line widely employed as a human model in carcinogenesis studies. In addition, colon cancer is a representative malignancy efficiently treated with Food and Drug Administration (FDA)-approved

and investigational drugs for phototherapy.²⁴ Cells were exposed to increasing concentrations of tested compounds (12 nM–200 μ M), and after 24 h, they were either irradiated at 360 nm for 30 min at 37 °C or kept in the dark. After an additional 24 h, cell damage was assessed by a MTT assay. Results were reported as the effective drug concentration able to kill 50% of the cell population after photoirradiation (EC_{50}) and the cytotoxic concentration that killed 50% of cell population without photoirradiation (CC_{50}). Selectivity indexes (SI) were measured as the ratio of CC_{50} over EC_{50} values. As shown in Table 2, three of nine compounds showed EC_{50} in the nanomolar range. In particular, the most active compound was BINOL derivative **8**, with an EC_{50} of 130 ± 40 nM. However, it also showed cytotoxicity prior to UV irradiation at doses of 14.00 ± 6.00 μ M (SI = 108). Compounds (*S,S,S*)-**5** and (*R,S,S*)-**5** were slightly less active, displaying EC_{50} of 220 ± 50 and 230 ± 20 nM, respectively, although they did not show cytotoxicity without irradiation up to 200 μ M (SI > 860). Once again, chiral properties did not confer appreciably different biological activities. The BINOLAM **7** exhibited EC_{50} in the low micromolar range (4.00 ± 0.08 μ M), yet it resulted even more cytotoxic without UV treatment (CC_{50} of 1.50 ± 0.02 μ M, SI = 0.4). Finally, BINOL derivatives (*S*)-**3b**, (*R*)-**3b**, (*S,S,S*)-**6**, (*R,S,S*)-**6**, and **10** did not show either photocytotoxic or cytotoxic effects at doses as high as 200 μ M. PS, used as a control, in these conditions displayed EC_{50} of 940 ± 90 nM and $CC_{50} > 200$ μ M.

Cellular drug effects depend upon not only selective target recognition but also the ability of the compound to enter the cell compartment through the plasmatic membrane. This property is usually theoretically and experimentally defined as log D (D = distribution), which is largely related to the compound hydrophobic/hydrophilic characteristics, expressed as log P (P stands for partitioning in *n*-octanol/water). Theoretical log P values for the neutral forms of tested BINOL–QMs were calculated according to the Crippen's fragmentation method (Table 2).²⁵ BINOL–amino acid conjugates **6** and **10** showed the lowest log P calculated on their neutral structure. In addition, the pI for compound **6**, roughly evaluated from the pI of their conjugated amino acids (pI 6.30, for proline), suggest that it should be mainly negatively charged, at pH 7.5. Similar consideration holds for compound **10**, suggesting that it should be mainly positively charged, at the working pH. Obviously, compound **3b** is permanently charged. Therefore, the access of **3b**, **6**, and **10** to the intracellular environment results severely hindered, as proven by the inability to induce either photocytotoxicity or cytotoxicity (Table 2). In contrast, BINOLAMs **5**, **7**, and **8** are only partially charged at physiological pH, and the neutral forms can diversely permeate according to their hydrophobic properties. This statement is supported by the fact that a hydroxyl group in *ortho* to a dimethylaminomethyl moiety reduces the basicity of the amino group (i.e., 2-dimethylaminomethyl-phenols pK_{a1} , 8.1; benzyl-dimethyl-amine pK_a , 9.1). For the BINOLAMs **5**, **7**, and **8**, we found a correlation between log P values and photocytotoxicity (**8** > **5** > **7**) (Table 2).

Hence, amino acid methyl esters appear to be most suitable for increasing cell-killing activity. In addition, the scale of photocytotoxicity soundly correlates with the ability to induce DNA XL (**8** > **5** > **7**), even though with different potency (nanomolar versus micromolar range, respectively). This biased active concentration range of results *in vitro* and, in the cells, may rest on a number of reasons: (1) cellular enzymes may metabolize the original compound enhancing its potency; (2) additional drug target(s) may be present in the cell environment,

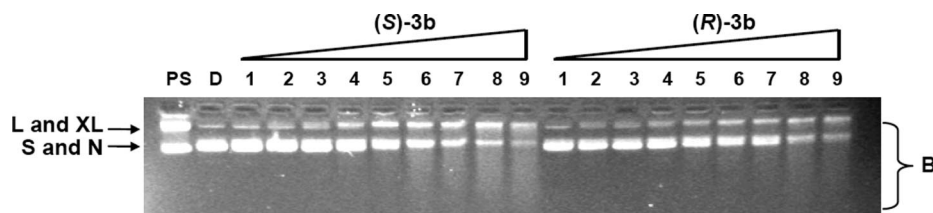


Figure 4. Concentration-dependent DNA-strand scission of BINOL–amino acid conjugates. Plasmid DNA was mixed with increasing amounts (0.62, 1.25, 2.5, 5, 10, 20, 40, 80, and 160 μM , lanes 1–9) of compound (S)-3b and (R)-3b (shown above the gel image), in phosphate buffer (50 mM, pH 7.5). Reaction mixtures were irradiated at 360 nm for 20 min, incubated for 24 h in alkaline-loading buffer, and loaded on 1% alkaline agarose gel. Gels were stained with ethidium bromide. Lane D is nontreated, irradiated DNA. Lane PS is a control for XL species induced by 4,5',8-trimethylpsoralen at 360 nm. Nonreacted forms of plasmid are indicated as S, N, and L. XL species are indicated as XL, on the left of the gel image. DNA breaks resulting in smeared bands are indicated as B.

thus producing synergistic effects; and (3) even poor drug-induced cell damage may trigger a massive cellular response, which eventually leads to cell death. An additional interesting feature can be inferred from our results: the L-proline methyl ester derivative stands out as the most promising Y group since BINOL derivative **5**, unlike L-alanine and L-valine derivatives, resulted highly photoselective, displaying cytotoxic effects only upon UV activation.

BINOLAMs Produce DNA Alkylation in Cell Systems. To test the ability of the BINOL–L-proline methyl ester to form DNA adducts in the cellular environment, we performed an alkaline comet assay.²⁶ LoVo cells were treated with increasing concentrations of compound (S,S,S)-5 (5–80 μM) and with PS as a positive control, as described in the photocytotoxicity experiments. After standard additional incubation for 24 h at 37 °C, cells were scraped off and suspended in low-melting agarose. After alkaline-induced lysis, cells were subjected to electrophoresis within the agarose gel, stained, and visualized by fluorescence microscopy. DNA damage was quantified, as described previously.²⁷ A minimum of 50 cells per sample were examined, and the damage extent for each cells was scored 0–4 “units of DNA damage” (UDD) as follows: 0, no damage, no DNA migration; 1, dense nucleus with slight migration of nuclear material; 2, the comet tail has progressed to its full length, but the comet width does not exceed that of the nucleus; 3, the comet tail is greater than the width of the nucleus, and the nucleus is less dense; 4, the nucleus and the tail are completely separated. From a comparison to the blank control, shorter tails indicate cross-linking and longer tails testify to DNA breaks. Representative images per each sample are shown in Figure 5a; results are reported as the medium value of damage extent for each sample (Figure 5b). The blank controls, before and after UV irradiation, exhibited only a slight comet tail, calculated as 1.15 and 1.30 UDD, respectively. When cells were treated with an increasing concentration of BINOLAM, the tail length and width gradually increased, indicating an enhanced DNA damage. The extent of nucleic acid breaks reached a maximum at 40 μM of drug concentration (2.94 UDD), after which the comet tail abode a minor decrease (2.80 UDD at 80 μM) (Figure 5b).

However, at increasing BINOLAM concentrations, the increased DNA damage was balanced by a higher number of cells displaying a shorter comet tail. This is evidenced both by cell images (see arrows pointing to less damaged cells in Figure 5a) and by the increased standard deviation obtained for higher values of drug concentrations (Figure 5b). Control cells treated with PS displayed a very consistent absence of the comet tail, indicating efficient cross-linking of the nucleic acid. These results indicate, first, that BINOLAMs reach their target DNA inside the cells and, second, that at low doses they alkylate chromosomal DNA, which, under alkaline conditions, undergoes strand scission. However, at higher concentrations, BINOLAMs

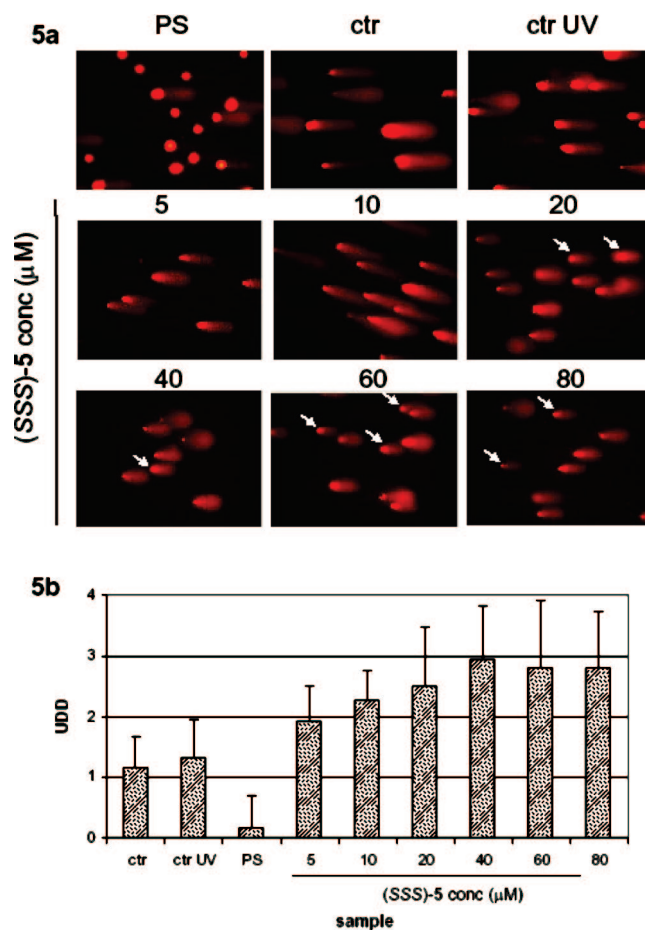


Figure 5. Alkaline comet assay for LoVo cell treated with compound (S,S,S)-5. (a) Cells were exposed to increasing concentrations of compound (S,S,S)-5 and irradiated at 360 nm for 30 min. Successively, they were suspended in low-melting agarose gel, subjected to electrophoresis within the agarose gel, stained, and visualized by fluorescence microscopy. A minimum of 50 cells per sample was analyzed. Arrows point to less damaged cells within each (S,S,S)-5-treated sample. (b) Length and shape of the comet tail were converted in UDD (units of DNA damage, see the text and Experimental Section for details). Results were reported as the medium of UDD per sample. ctr and ctr UV indicate blank controls, before and after UV irradiation, respectively.

display increased cross-linking ability, which reflects the wider range of tail lengths obtained in the comet assay.

Conclusions

The production of bis-alkylating BINOL–QMs starting from quaternary ammonium salts and their DNA cross-linking properties was previously demonstrated.^{7b} Now, the photoge-

neration of related transient electrophiles has been achieved in excellent quantum yields using BINOL–amino acid and –amino ester derivatives as the precursors. QM-trapping experiments show that bis-alkylation is the result of the sequential generation of two monoalkylating BINOL–QMs. The majority of the BINOL–amino acid and –amino ester precursors, when photoactivated at 360 nm in the presence of supercoiled plasmid DNA (pBR322), displayed DNA cross-linking potency comparable to that of the quaternary ammonium salts (range of 1–5 μ M). Unlike the latter, the amino acid methyl esters exhibit potent photocytotoxicity against the human colorectal adenocarcinoma LoVo cell line in the nanomolar concentration range (130–230 nM). Among the 3,3'-CH₂Y-disubstituted BINOLs tested, the L-proline methyl ester congener stands out as the most promising lead because, contrary to other derivatives, it showed remarkably high photoselectivity, displaying prominent cell killing effects only after UV irradiation. In this connection, it is worth recalling that PS, one of the most effective phototoxic agents thus far reported, is about 4 times less potent than our newly tested compounds. In addition, we have shown that BINOLAMs efficiently reach their DNA target inside the cells. However, their mechanism of action differs to some extent from that of a photoactivable reference drug, such as PS. In fact, we have displayed that the photogenerated QMs inside the cells exhibit mono- and bis-alkylating properties, resulting in DNA scission and cross-linking. Analysis of DNA sequence specificity and alkylation product characterization represent the next step toward the development of potent photocytotoxic-selective compounds.

Experimental Section

General Procedures. The BINOLs **2b** and **3b**,^{7b,26} the dialdehyde **11**,^{20,28} and the dibromide **12**²⁹ have been synthesized according to published procedures. The diastereomerically pure (*S,S,S*)- and (*R,S,S*) BINOL–esters **4** and **5** have been previously synthesized and characterized.^{7c} The alkylation adducts **13** and **14** were purified and characterized by a comparison to authentic samples.^{7b}

General Reductive Amination for the Synthesis of 4, 5, and 7–9. The followed procedure is a modified version that is already published.¹⁹ A suspension of L-amino-ester HCl (5 mmol) in CH₂Cl₂ (25 mL) was added to a CH₂Cl₂ solution of Et₃N (1 mL). The solution was stirred at room temperature for 1 h, and then a solution of dialdehyde **11** (700 mg, 2 mmol) in CH₂Cl₂ was added together with molecular sieves at 4 Å. This solution was stirred under nitrogen atmosphere, at room temperature. After 16 h, NaBH(OAc)₃ (880 mg, 4 mmol) was added. The resulting suspension was further stirred for another 3 h at room temperature, under an inert atmosphere. At this time, a solution of Na₂CO₃ was added to the mixture, then the organic layer was separated, and the residual solution was extract twice with CH₂Cl₂.

The mixture of the reaction has been separated by silica-gel column chromatography, eluting with 7:3 cyclohexane/ethylacetate.

Synthesis of 6 and 10 by Deprotection of 4 and 9: General Procedure.²¹ The *t*-butyl amino ester (1 mmol) was deprotected by dissolving it in a solution of trifluoroacetic acid (1.94 mL, 13 mmol) and dichloromethane (10 mL) in the presence of triethylsilane (0.8 mL, 2.5 mmol), at room temperature. After stirring for 25 min, 1 M HCl (1 mL) was added and the solvent was removed in vacuo. The residue was suspended in diethyl ether, and the product was isolated by filtration. The yields were almost quantitative (93%), only using triethylsilane as the carbocation scavenger.

3,3'-Bis-(2-carboxypyrrolidin-1-ylmetil)-1,1'-dinaphtyl-2,2'-diolo·2HCl (6). (*S,S,S*)-**6** 2HCl. White crystals. mp > 180 °C (dec.). ¹H NMR (D₂O) δ : 1.85 (broad s, 2 H), 2.01 (broad s, 4 H), 2.41 (broad s, 2 H), 3.25 (broad s, 2 H), 3.59 (broad s, 2 H), 4.18 (broad s, 2 H), 4.40 (d, 2 H, *J* = 11.3 Hz), 4.55 (d, 2 H, *J* = 11.3),

6.56 (broad s, 2 H), 6.68 (broad s, 2 H), 7.10 (broad s, 2 H), 7.77 (broad s, 2 H), 7.96 (broad s, 2 H). ¹H NMR (DMSO-*d*₆) δ : 1.95–2.11 (m, 6 H), 2.43–2.51 (m, 2 H), 3.38–3.41 (m, 2 H), 3.62–3.75 (m, 2 H), 4.47–4.52 (m, 2 H), 4.56–4.79 (m, 4 H), 6.93–7.01 (m, 2 H), 7.21–7.30 (m, 2 H), 7.32–7.38 (m, 2 H), 7.92 (dd, 2 H, *J* = 4.0, *J* = 7.8 Hz), 8.14 (d, 2 H, *J* = 7.5 Hz). ¹³C NMR (D₂O) δ : 22.54 (CH₂), 28.42 (CH₂), 54.80 (CH₂), 55.07 (CH₂), 67.06 (CH), 113.23 (C), 119.33 (C), 123.47 (CH), 124.34 (CH), 128.08 (C), 128.12 (CH), 128.66 (CH), 134.03 (CH), 134.34 (C), 151.13 (C), 171.85 (C). Anal. Calcd (C₃₂H₃₄Cl₂N₂O₆): C, H, Cl, N.

(*R,S,S*)-6·2HCl. White crystals. mp > 177 °C (dec.). ¹H NMR (D₂O) δ : 1.82 (broad s, 2 H), 2.05 (broad s, 4 H), 2.44 (broad s, 2 H), 3.25 (broad s, 2 H), 3.62 (broad s, 2 H), 4.17 (broad s, 2 H), 4.42 (d, 2 H, *J* = 11.3 Hz), 4.58 (d, 2 H, *J* = 11.3), 6.59 (broad s, 2 H), 6.70 (broad s, 2 H), 7.12 (broad s, 2 H), 7.80 (broad s, 2 H), 8.01 (broad s, 2 H). ¹³C NMR (D₂O) δ : 22.60 (CH₂), 28.55 (CH₂), 54.81 (CH₂), 55.17 (CH₂), 67.12 (CH), 113.33 (C), 119.37 (C), 123.57 (CH), 124.37 (CH), 128.00 (C), 128.22 (CH), 128.69 (CH), 134.06 (CH), 134.39 (C), 151.17 (C), 171.89 (C). Anal. Calcd (C₃₂H₃₄Cl₂N₂O₆): C, H, Cl, N.

7. Equimolar diastereomeric mixture. Yellow oil. ¹H NMR (CDCl₃) δ : 1.25–1.45 (s, 6 H), 3.25–3.75 (m, 2 H), 3.8 (s, 6 H), 4.00–4.15 (m, 2 H), 4.25–4.45 (m, 2 H), 7.10–7.35 (m, 6 H), 7.70–7.90 (m, 4 H). ¹³C NMR (CDCl₃) δ : 18.84 (CH₃), 51.31 (CH₂), 52.10 (CH), 55.40 (CH₃), 123.06 (CH), 124.7(CH), 126.1 (CH), 127.7 (CH), 127.9 (CH), 133.65 (C), 153.18 (C), 174.77 (C). Anal. Calcd (C₃₀H₃₂N₂O₆): C, H, N.

8. Equimolar diastereomeric mixture. Yellow oil. ¹H NMR (CDCl₃) δ : 1.25–1.45 (s, 12 H), 3.10–3.25 (m, 2 H), 3.65–3.80 (m, 2 H), 3.85 (s, 6 H), 3.90–4.35 (m, 4 H), 7.10–7.35 (m, 6 H), 7.70–7.90 (m, 4 H). ¹³C NMR (CDCl₃) δ : 18.97 (CH₃), 51.81 (CH₂), 51.93 (CH), 60.31 (CH₃), 123.06 (CH), 124.7(CH), 126.1 (CH), 127.7 (CH), 127.9 (CH), 133.45 (C), 154.08 (C), 174.13 (C). Anal. Calcd (C₃₄H₄₀N₂O₆): C, H, N.

9. The compound was not characterized by NMR and used for the further step in the synthesis of **10**.

10. Equimolar diastereomeric mixture. Yellow oil. ¹H NMR (D₂O) δ : 1.30–2.10 (m, 12 H), 2.60–3.10 (m, 4 H), 3.75–3.95 (m, 2 H), 4.25–4.65 (m, 4 H), 6.90–7.00 (m, 2 H), 7.20–7.40 (m, 4 H), 7.80–8.15 (m, 4 H). ¹³C NMR (D₂O) δ : 21.49 (CH₂), 24.80 (CH₂), 26.25 (CH₂), 28.73 (CH₂), 28.89 (CH₂), 29.19 (CH₂), 38.92 (CH₂), 46.52 (CH₂), 47.02 (CH₂), 47.47 (CH₂), 48.81 (CH), 52.74 (CH), 113.62 (C), 113.69 (C), 123.75 (CH), 123.81 (CH), 124.59 (CH), 128.3 (CH), 128.45 (C), 128.66 (C), 128.71 (CH), 133.0 (CH), 133.5 (CH), 133.6 (CH), 134.35 (C), 134.5 (C), 151.16 (C), 151.30 (C), 171.79 (C), 171.89 (C). Anal. Calcd (C₃₄H₄₄Cl₂N₄O₆): C, H, Cl, N.

(*S,S*)-15·HCl. Yellow oil. ¹H NMR (D₂O) δ : 1.55–1.75 (m, 2 H), 2.15–2.22 (m, 1 H), 2.28–2.45 (m, 1 H), 2.48–2.60 (m, 1 H), 3.15–3.25 (m, 1 H), 3.65–3.80 (m, 1 H), 3.85 (d, 1 H, *J* = 13.2), 4.60 (d, 1 H, *J* = 13.2), 5.60 (m, 2 H), 5.70 (m, 1 H, acid), 7.20–7.30 (m, 4 H), 7.30–7.40 (m, 2 H), 7.55–7.70 (m, 4 H), 8.50 (s, 2 H, acid). ¹³C NMR (C₅D₅N) δ : 23.39 (CH₂), 29.93 (CH₂), 53.14 (CH₂), 57.27 (CH₂), 61.39 (CH₂), 66.25 (CH), 116.09 (C), 116.34 (C), 125.44 (CH), 125.84 (CH), 126.27 (CH), 126.43 (CH), 126.48 (CH), 126.61 (CH), 128.32 (CH), 128.89 (CH), 128.96 (CH), 129.26 (CH), 133.05 (C), 134.41 (C), 153.07 (C), 155.23 (C), 176.15 (C). Anal. Calcd (C₂₇H₂₆ClNO₅): C, H, Cl, N.

(*R,S*)-15·HCl. Yellow oil. ¹H NMR (C₅D₅N) δ : 1.60–1.80 (m, 2 H), 2.05–2.20 (m, 1 H), 2.25–2.40 (m, 1 H), 2.48–2.60 (m, 1 H), 3.00–3.15 (m, 1 H), 3.65–3.80 (m, 1 H), 3.90 (d, 1 H, *J* = 13.2), 4.82 (d, 1 H, *J* = 13.2), 5.62 (m, 2 H), 5.70 (m, 1 H, acid), 7.20–7.30 (m, 4 H), 7.30–7.40 (m, 2 H), 7.55–7.70 (m, 4 H), 8.50 (s, 2 H, acid). ¹³C NMR (C₅D₅N) δ : 23.39 (CH₂), 29.93 (CH₂), 53.14 (CH₂), 57.27 (CH₂), 61.39 (CH₂), 66.25 (CH), 116.09 (C), 116.34 (C), 125.44 (CH), 125.84 (CH), 126.27 (CH), 126.43 (CH), 126.48 (CH), 126.61 (CH), 128.32 (CH), 128.89 (CH), 128.96 (CH), 129.26 (CH), 133.05 (C), 134.41 (C), 153.07 (C), 155.23 (C), 176.15 (C). Anal. Calcd (C₂₇H₂₆ClNO₅): C, H, Cl, N.

(S,S)-16. Yellow oil. ^1H NMR (CD_3OD) δ : 1.25–1.35 (m, 9 H), 1.75–2.00 (m, 3 H), 2.25–2.40 (m, 1 H), 2.60–2.80 (m, 1 H), 3.20–3.35 (m, 1 H), 3.45–3.55 (m, 1 H), 4.18 (d, 2 H, $J = 13.2$ Hz), 4.30 (d, 2 H, $J = 13.2$ Hz), 4.95 (s, 2 H), 6.80–7.00 (m, 2 H), 7.00–7.30 (m, 4 H), 7.75–7.85 (m, 3 H), 7.95 (s, 1 H). ^{13}C NMR (MeOD) δ : 24.39 (CH_2), 28.41 (CH_3), 32.13 (CH_2), 54.89 (CH_2), 58.63 (CH_2), 62.24 (CH_2), 68.02 (CH), 83.85 (C), 115.95 (C), 116.34 (C), 124.38 (CH), 124.64 (CH), 125.89 (CH), 126.05 (CH), 127.09 (CH), 127.84 (CH), 128.05 (CH), 130.63 (CH), 130.91 (CH), 131.71 (CH), 135.21 (C), 136.17 (C), 152.59 (C), 155.16 (C), 173.91 (C). Anal. Calcd ($\text{C}_{31}\text{H}_{33}\text{NO}_5$): C, H, N.

(R,S)-16. Yellow oil. ^1H NMR (CD_3OD) δ : 1.15–1.20 (m, 9 H), 1.80–2.05 (m, 2 H), 2.20–2.30 (m, 2 H), 2.72–2.87 (m, 2 H), 3.40–3.55 (m, 1 H), 4.15 (d, 2 H, $J = 13.2$ Hz), 4.50 (d, 2 H, $J = 13.2$ Hz), 4.95 (s, 2 H), 6.80–7.00 (m, 2 H), 7.00–7.30 (m, 4 H), 7.75–7.85 (m, 3 H), 7.95 (s, 1 H). ^{13}C NMR (MeOD) δ : 24.39 (CH_2), 28.41 (CH_3), 32.13 (CH_2), 54.89 (CH_2), 58.63 (CH_2), 62.24 (CH_2), 68.02 (CH), 83.85 (C), 115.95 (C), 116.34 (C), 124.38 (CH), 124.64 (CH), 125.89 (CH), 126.05 (CH), 127.09 (CH), 127.84 (CH), 128.05 (CH), 130.63 (CH), 130.91 (CH), 131.71 (CH), 135.21 (C), 136.17 (C), 152.59 (C), 155.16 (C), 173.91 (C). Anal. Calcd ($\text{C}_{31}\text{H}_{33}\text{NO}_5$): C, H, N.

Cross-Linking of Plasmid DNA. Compounds (*S*)-**3b**, (*R*)-**3b**, (*S,S,S*)-**5**, (*R,S,S*)-**5**, (*S,S,S*)-**6**, (*R,S,S*)-**6**, **7**, **8**, and **10** were dissolved in DMSO to a final concentration of 20 mM. These stock solutions were diluted in mQ-grade H_2O and used for reactions. Plasmid pBR322 (0.5 $\mu\text{g}/\text{sample}$) was mixed with increasing amounts (0.62, 1.25, 2.5, 5, 10, 20, 40, and 80 μM , as indicated in each figure) of each compound, in phosphate buffer (50 mM, pH 7.5). For pH-dependent experiments, QMs at 20 μM doses were reacted with pBR322 in 50 mM phosphate buffer at pH 5.5, 6.5, 7.5, and 8.5. A saturated water solution of PS was used to get a 0.5 μM concentration of drug in the control samples. Reaction mixtures were irradiated on ice for 20 min at 360 nm at 120 W in a photochemical multirays reactor (Helios Italquartz, Italy). Irradiated solutions were added to alkaline agarose gel loading buffer [50 mM NaOH, 1 mM ethylenediaminetetraacetic acid (EDTA), 3% Ficoll, and 0.02% bromophenol blue] and loaded on a 1% alkaline agarose gel containing 50 mM NaOH and 1 mM EDTA. Gels were run in 50 mM NaOH and 1 mM EDTA at 12 V for 15–16 h, stained with ethidium bromide (0.5 $\mu\text{g}/\text{mL}$) for 10 min, and subsequently washed in water for 10 min. Stained gels were visualized in Gel-Doc 1000 (Bio-Rad, Italy), and DNA bands were quantified by Quantity One software (Bio-Rad).

Photocytotoxicity and Cytotoxicity Assays. Human colorectal adenocarcinoma cells (LoVo) were a kind gift of Dr. C. Marzano, Department of Pharmaceutical Sciences, University of Padova, Italy. LoVo cells were grown as monolayers in Dulbecco's Modified Eagle Medium/F-12 nutrient mixture (D-MEM/F-12) 1:1 mixture (Invitrogen, Italy) with 10% fetal bovine serum (FBS) supplemented with penicillin (100 units/mL) and streptomycin (100 $\mu\text{g}/\text{mL}$) in a humidified atmosphere with 5% CO_2 at 37 $^\circ\text{C}$.

Cytotoxic effects on tumor cell growth were determined by a MTT assay. QM compounds and TMP were dissolved and diluted into working concentrations with DMSO. Cells (1.75×10^4 cells/well) were plated onto 96-microwell plates to a final volume of 100 μL and allowed an overnight period for attachment. At day 1, 1 μL of each dilution of tested compounds was added per well to get a 1% final concentration of drug solvent per well; at day 2, medium was removed, cells washed with phosphate-buffered saline (PBS), and fresh medium was added. Immediately after, QM- and TMP-treated cells were irradiated for 30 min at 360 nm in a photochemical multirays reactor and incubated at 37 $^\circ\text{C}$ for an additional 24 h. Control cells (without any compound but with 1% drug solvent) were treated in the exact same conditions. Cell survival was evaluated by a MTT assay: 10 μL of freshly dissolved solution of MTT (5 mg/mL in PBS) were added to each well, and after 4 h of incubation, 100 μL of solubilization solution [10% sodium dodecyl sulfate (SDS) and 0.01 M HCl] were added. After overnight incubation at 37 $^\circ\text{C}$, absorbance was read at 540 nm. Data were expressed as mean values of three individual experiments

conducted in triplicate. The percentage of cell survival was calculated as follows: cell survival = $(A_{\text{well}} - A_{\text{blank}})/(A_{\text{control}} - A_{\text{blank}}) \times 100$, where blank denotes the medium without cells.

Alkaline Comet Assay. Cross-link formation and DNA damage were determined by the alkaline comet assay.²⁶ Human colorectal adenocarcinoma cells (LoVo) were plated (4×10^5 cells/well) onto 6-well plates to a final volume of 2 mL and allowed an overnight period for attachment. At day 1, medium was removed and replaced with medium containing compound (*S,S,S*)-**5** at working dilutions to get a 1% final DMSO concentration per well; at day 2, medium was removed, cells washed with PBS, and fresh medium was added. Immediately after, cells were irradiated for 30 min at 360 nm in a photochemical multirays reactor and incubated at 37 $^\circ\text{C}$ for an additional 24 h. Control cells (without compound but with 1% DMSO) were treated in the exact same conditions. After 24 h of incubation, medium was removed and replaced with mincing solution (HBSS Ca^{2+} , Mg^{2+} free, 20 mM EDTA, 10% DMSO) and cells were scraped off and resuspended to get approximately 2×10^6 cells/mL. A total of 10 μL of cells were suspended in 65 μL of 0.5% low-melting point agarose and dispensed onto a clear microscope slide precoated with 1% normal melting point agarose (air dried). Cells were lysed overnight at 4 $^\circ\text{C}$ in cold lysis buffer (2.5 M NaCl, 100 mM EDTA, and 10 mM Tris-HCl at pH 10.0) containing freshly added 1% Triton X-100. Slides were then washed in Tris and incubated in alkaline electrophoresis buffer (300 mM NaOH and 1 mM EDTA at pH > 13) for 30 min, followed by electrophoresis in the same buffer at 12 V and 300 mA for 40 min. Slides were then rinsed with neutralization buffer (0.4 M Tris at pH 7.5) and left to air dry. All procedures were carried out under dim yellow light. After drying, slides were stained with 75 μL of a 10 $\mu\text{g}/\text{mL}$ stock solution of propidium iodide and incubated for 20 min. Images were analyzed using a Leica fluorescence microscope DM4500B, with an excitation filter of 515–560 nm and a barrier filter of 590 nm, at 20 \times magnification. Images were captured by an online charge-coupled device (CCD) camera Leica DFC480.

DNA damage was quantitated after electrophoresis of slides as described previously.²⁷ A minimum of 50 cells per sample were examined, and the extent of damage to each cell was assigned a score of 0–4 as follows: 0, no damage, no DNA migration; 1, dense nucleus with slight migration of nuclear material; 2, the comet tail has progressed to its full length, but the comet width does not exceed that of the nucleus; 3, the comet tail is greater than the width of the nucleus, and the nucleus is less dense; 4, the nucleus and the tail are completely separated.

Acknowledgment. This research was supported in part by Pavia University (Grant FAR 2005) and "Consorzio CINMPIS". We also thank Prof. Remo Gandolfi for helpful discussions.

Supporting Information Available: ^1H and ^{13}C NMR for **4**, **5**, and **11**, experimental general procedures, and preparative photolysis of BINOLAMs in the presence of water, morpholine, and 2-mercaptoethanol. This material is available free of charge via the Internet at <http://pubs.acs.org>.

References

- (1) (a) Noll, D. M.; Mason, T. M.; Miller, P. S. Formation and Repair of Interstrand Cross-Links in DNA. *Chem. Rev.* **2006**, *106*, 277–301. (b) Rajsiki, S. R.; Williams, R. M. DNA Cross-Linking Agents as Antitumor Drugs. *Chem. Rev.* **1998**, *98*, 2723–2795. (c) Dervan, P. B. Design of Sequence-Specific DNA-Binding Molecules. *Science* **1986**, *232*, 464–471. (d) Sigman, D. S.; Mazumder, A.; Perrin, D. M. Chemical Nucleases. *Chem. Rev.* **1993**, *93*, 2295–2316.
- (2) (a) Gniazdowski, M.; Cera, C. The Effects of DNA Covalent Adducts on in Vitro Transcription. *Chem. Rev.* **1996**, *96*, 619–634. (b) Kohn, K. W. In *Topics in Structural and Molecular Biology: 3. Molecular Aspects of Anti-cancer Drug Action*; Neidle, S., Waring, M., Eds.; Verlag Chemie: Weinheim, Germany, 1994; Vol. 315, p 330. (c) Lippard, S. J.; Kane, S. A. Photoreactivity of Platinum(II) in Cisplatin-Modified DNA Affords Specific Cross-Links to HMG Domain Proteins. *Biochemistry* **1996**, *35*, 2180–2188.
- (3) Kolkenberg, S. E.; Boger, D. L. Mechanisms of in Situ Activation for DNA-Targeting Antitumor Agents. *Chem. Rev.* **2002**, *102*, 2477–2495.

- (4) Saito, I.; Nakatani, K. Design of DNA-Cleaving Agents. *Bull. Chem. Soc. Jpn.* **1996**, *69*, 3007–3019.
- (5) Chatterjee, M.; Rokita, S. E. The Role of a Quinone Methide in the Sequence Specific Alkylation of DNA. *J. Am. Chem. Soc.* **1994**, *116*, 1690–1697.
- (6) (a) Woo, J.; Hopkins, P. B. Template-Directed Modification of Single-Stranded DNA by Psoralen-Tethered Oligonucleotides: Sites of Photoadduct Formation Analyzed by Sequence-Specific and Sequence-Random Cleavage. *J. Am. Chem. Soc.* **1991**, *113*, 5457–5459. (b) Straub, K.; Kanne, D.; Hearst, J. E.; Rapoport, H. Isolation and Characterization of Pyrimidine–Psoralen Photoadducts from DNA. *J. Am. Chem. Soc.* **1981**, *103*, 2347–2355. (c) Sastry, S. S.; Spielmann, P. H.; Hoang, Q. S.; Phillips, A. M.; Sancar, A.; Hearst, J. H. Laser-Induced Protein–DNA Cross-Links via Psoralen Furanside Monoadducts. *Biochemistry* **1993**, *32*, 5526–5538.
- (7) (a) Modica, E.; Zanaletti, R.; Freccero, M.; Mella, M. Alkylation of Amino Acids and Glutathione in Water by *o*-Quinone Methide. Reactivity and Selectivity. *J. Org. Chem.* **2001**, *66*, 41–52. (b) Richter, S.; Maggi, S.; Colloredo-Mels, S.; Palumbo, M.; Freccero, M. Binol Quinone Methides as Bisalkylating and DNA Cross-Linking Agents. *J. Am. Chem. Soc.* **2004**, *126*, 13973–13979. (c) Colloredo-Mels, S.; Doria, F.; Verga, D.; Freccero, M. Photogenerated Quinone Methides as Useful Intermediates in the Synthesis of Chiral BINOL Ligands. *J. Org. Chem.* **2006**, *71*, 3889–3895. (d) Verga, D.; Richter, S. N.; Palumbo, M.; Gandolfi, R.; Freccero, M. Bipyridyl Ligands as Photoactivatable Mono- and Bis-alkylating Agents Capable of DNA Cross-Linking. *Org. Biomol. Chem.* **2007**, *5* (2), 233–235. (e) Freccero, M. Quinone Methides as Alkylating and Cross-Linking Agents. *Mini-Rev. Org. Chem.* **2004**, *1*, 403–415.
- (8) (a) Diao, L.; Cheng, Y.; Wan, P. Quinone Methide Intermediates from the Photolysis of Hydroxybenzyl Alcohols in Aqueous Solution. *J. Am. Chem. Soc.* **1995**, *117*, 5369–5370. (b) Brousmiche, D.; Wan, P. Photogeneration of an *o*-Quinone Methide from Pyridoxine (Vitamin B₆) in Aqueous Solution. *Chem. Commun.* **1998**, 491–492.
- (9) (a) Chiang, Y.; Kresge, A. J.; Zhu, Y. Flash Photolytic Generation and Study of *p*-Quinone Methide in Aqueous Solution. An Estimate of Rate and Equilibrium Constants for Heterolysis of the Carbon–Bromine Bond in *p*-Hydroxybenzyl Bromide. *J. Am. Chem. Soc.* **2002**, *123*, 6349–6356. (b) Chiang, Y.; Kresge, A. J.; Zhu, Y. Flash Photolytic Generation of *o*-Quinone-phenylmethide and *o*-Quinone-(*p*-anisyl) methide in Aqueous Solution and Investigation of Their Reactions in That Medium. Saturation of Acid-Catalyzed Hydration. *J. Am. Chem. Soc.* **2002**, *123*, 717–722. (c) Chiang, Y.; Kresge, A. J.; Zhu, Y. Flash Photolytic Generation of *ortho*-Quinone Methide in Aqueous Solution and Study of Its Chemistry in That Medium. *J. Am. Chem. Soc.* **2001**, *123*, 8089–8094.
- (10) Nakatani, K.; Higashida, N.; Saito, I. Highly Efficient Photochemical Generation of *o*-Quinone Methide from Mannich Bases of Phenol Derivatives. *Tetrahedron Lett.* **1997**, *38*, 5005–5008.
- (11) Yang, J.; Pande, P.; Shearer, J.; Greenberg, W. A.; Zeng, Q.; Rokita, S. E. Quinone Methide Alkylation of Deoxycytidine. *J. Org. Chem.* **1997**, *62*, 3010–3012.
- (12) (a) Veldhuyzen, W. F.; Shalloo, A. J.; Jones, R. A.; Rokita, S. E. Thermodynamic versus Kinetic Products of DNA Alkylation as Modeled by Reaction of Deoxyadenosine. *J. Am. Chem. Soc.* **2001**, *123*, 11126–11132. (b) Pande, P.; Shearer, J.; Yang, J.; Greenberg, W. A.; Rokita, S. E. Alkylation of Nucleic Acids by a Model Quinone Methide. *J. Am. Chem. Soc.* **1999**, *121*, 6773–6779.
- (13) Weinert, E. E.; Dondi, R.; Colloredo-Mels, S.; Frankenfield, K. N.; Mitchell, C. H.; Freccero, M.; Rokita, S. E. Substituents on Quinone Methides Strongly Modulate Formation and Stability of Their Nucleophilic Adducts. *J. Am. Chem. Soc.* **2006**, *128*, 11940–11947.
- (14) (a) Flegel, M.; Lukeman, M.; Huck, L.; Wan, P. Photoaddition of Water and Alcohols to the Anthracene Moiety of 9-(2'-Hydroxyphenyl)anthracene via Formal Excited State Intramolecular Proton Transfer. *J. Am. Chem. Soc.* **2004**, *126*, 7890–7897. (b) Brousmiche, D. W.; Xu, M.; Lukeman, M.; Wan, P. Photohydration and Photosolvolysis of Biphenyl Alkenes and Alcohols via Biphenyl Quinone Methide-Type Intermediates and Diarylmethyl Carbocations. *J. Am. Chem. Soc.* **2003**, *125*, 12961–12970. (c) Lukeman, M.; Wan, P. Excited-State Intramolecular Proton Transfer in *o*-Hydroxybiaryls: A New Route to Dihydroaromatic Compounds. *J. Am. Chem. Soc.* **2003**, *125*, 1164–1165. (d) Lukeman, M.; Wan, P. A New Type of Excited-State Intramolecular Proton Transfer: Proton Transfer from Phenol OH to a Carbon Atom of an Aromatic Ring Observed for 2-Phenylphenol. *J. Am. Chem. Soc.* **2002**, *124*, 9458–9464.
- (15) (a) Veldhuyzen, W. F.; Praveen, P.; Rokita, S. E. A Transient Product of DNA Alkylation Can Be Stabilized by Binding Localization. *J. Am. Chem. Soc.* **2003**, *125*, 14005–14013. (b) Wang, P.; Liu, R.; Wu, X.; Ma, H.; Cao, X.; Zhou, P.; Zhang, J.; Weng, X.; Zhang, X.-L.; Qi, J.; Zhou, X.; Weng, L. A. Potent, Water-Soluble and Photoinducible DNA Cross-Linking Agent. *J. Am. Chem. Soc.* **2003**, *125*, 1116–1117.
- (16) (a) Jarver, P.; Langel, U. The use of cell-penetrating peptides as a tool for gene regulation. *Drug Discovery Today* **2004**, *9*, 395–402. (b) Wagstaff, K. M.; Jans, D. A. Protein transduction: cell penetrating peptides and their therapeutic applications. *Curr. Med. Chem.* **2006**, *13*, 1371–1387. (c) Lundberg, P.; Langel, U. A brief introduction to cell-penetrating peptides. *J. Mol. Recognit.* **2003**, *16*, 227–233.
- (17) Kaihatsu, K.; Janowski, B. A.; Corey, D. R. Recognition of chromosomal DNA by PNAs. *Chem. Biol.* **2004**, *11*, 749–758.
- (18) (a) Shibasaki, M.; Matsunaga, S. Design and Application of Linked-BINOL Chiral Ligands in Bifunctional Asymmetric Catalysis. *Chem. Soc. Rev.* **2006**, *35*, 269–279. (b) Brunel, J. M. BINOL: A Versatile Chiral Reagent. *Chem. Rev.* **2005**, *105*, 857–897. (c) Chen, Y.; Yekta, S.; Yudin, A. K. Modified BINOL Ligands in Asymmetric Catalysis. *Chem. Rev.* **2003**, *103*, 3155–3211.
- (19) Abdel-Magid, A. F.; Kenneth, G.; Carson, B. D.; Cynthia, A. M.; Shah, R. D. Reductive Amination of Aldehydes and Ketones with Sodium Triacetoxyborohydride. Studies on Direct and Indirect Reductive Amination Procedures. *J. Org. Chem.* **1996**, *61*, 3849–3862.
- (20) Brunner, H.; Goldbrunner, J. Asymmetrische Katalysen, II: Optisch Aktive Binaphthyl-derivate—Synthese und Einsatz in Übergangsmetallkatalysatoren. *Chem. Ber.* **1989**, *122*, 2005–2009.
- (21) Mehta, A.; Jaouhari, R.; Benson, T. J.; Douglas, K. T. Improved Efficiency and Selectivity in Peptide Synthesis: Use of Trihydropyridylsilane as a Carbocation Scavenger in Deprotection of *t*-Butyl Esters and *t*-Butoxycarbonyl-Protected Sites. *Tetrahedron Lett.* **1992**, *33*, 5441–5444.
- (22) Musil, L.; Koutek, B.; Pisova, M.; Soucek, M. Delocalization and Stability of *o*- and *p*-Quinone Methides: A HMO Study. *Collect. Czech. Chem. Commun.* **1981**, *46*, 1148–1159.
- (23) Maxam, A. M.; Gilbert, W. Sequencing End-Labeled DNA with Base-Specific Chemical Cleavages. *Methods Enzymol.* **1980**, *65*, 499–560.
- (24) (a) Wang, J. B.; Liu, L. X. Use of Photodynamic Therapy in Malignant Lesions of Stomach, Bile Duct, Pancreas, Colon and Rectum. *Hepatogastroenterology* **2007**, *75*, 718–724. (b) Busch, T. M.; Hahn, S. M.; Wileyto, E. P.; Koch, C. J.; Fraker, D. L.; Zhang, P.; Putt, M.; Gleason, K.; Shin, D. B.; Emanuele, M. J.; Jenkins, K.; Glatstein, E.; Evans, S. M. Hypoxia and Photofrin Uptake in the Intraperitoneal Carcinomatosis and Sarcomatosis of Photodynamic Therapy Patients. *Clin. Cancer Res.* **2004**, *14*, 4630–4638. (c) Woodhams, J. H.; MacRobert, A. J.; Novelli, M.; Bown, S. G. Photodynamic Therapy with WST09 (Tookad): Quantitative Studies in Normal Colon and Transplanted Tumours. *Int. J. Cancer* **2006**, *2*, 477–482. (d) Hahn, S. M.; Putt, M. E.; Metz, J.; Shin, D. B.; Rickter, E.; Menon, C.; Smith, D.; Glatstein, E.; Fraker, D. L.; Busch, T. M. Photofrin Uptake in the Tumor and Normal Tissues of Patients Receiving Intraperitoneal Photodynamic Therapy. *Clin. Cancer Res.* **2006**, *18*, 5464–5470. (e) Zawacka-Pankau, J.; Issaeva, N.; Hossain, S.; Pramanik, A.; Selivanova, G.; Podhajska, A. J. Protoporphyrin IX Interacts with Wild-Type p53 Protein in Vitro and Induces Cell Death of Human Colon Cancer Cells in a p53-Dependent and -Independent Manner. *J. Biol. Chem.* **2007**, *4*, 2466–2472.
- (25) Ghose, A. K.; Crippen, J. M. Atomic Physicochemical Parameters for Three-Dimensional Structure-Directed Quantitative Structure–Activity Relationships. 2. Modeling Dispersive and Hydrophobic Interactions. *J. Chem. Inf. Comput. Sci.* **1987**, *27*, 21–35.
- (26) Singh, N. P.; McCoy, M. T.; Tice, R. R.; Schneider, E. L. A Simple Technique for Quantitation of Low Levels of DNA Damage in Individual Cells. *Exp. Cell Res.* **1988**, *175*, 184–191.
- (27) Collins, A. R.; Ma, A. G.; Duthie, S. J. The Kinetics of Repair of Oxidative DNA Damage (Strand Breaks and Oxidised Pyrimidines) in Human Cells. *Mutat. Res.* **1995**, *336*, 69–77.
- (28) Moneta, W.; Baret, P.; Pierre, J.-L. Synthèses de récepteurs Macro-cycliques Contenant des Groupements Hydroxyls ou Métoxyyles Convergents, dans une Géométrie Définie, Effet de Matrice du Bore. *Bull. Soc. Chim. Fr.* **1988**, *6*, 995–1004.
- (29) Cram, D. J.; Helgeson, C.; Peacock, C.; Kaplan, L.; Domeier, L.; Moreau, P.; Koga, K.; Mayer, J.; Chao, Y.; Siegel, M.; Hoffmann, D.; Sogah, G. D. Y. Host–Guest Complexation. 8. Macrocyclic Polyethers Shaped by Two Rigid Substituted Dinaphthyl or Ditetralyl Units. *J. Org. Chem.* **1978**, *43*, 1930–1946.